

MultiModalPFN: Extending Prior-Data Fitted Networks for Multimodal Tabular Learning*

Wall Kim
Samsung Electronics
Hwaseong, South Korea
wall.kim@samsung.com

Chaeyoung Song Hanul Kim
Seoul National University of Science and Technology
Seoul, South Korea
{cy.song, hukim}@seoultech.ac.kr

Abstract

Recently, TabPFN has gained attention as a foundation model for tabular data. However, it struggles to integrate heterogeneous modalities such as images and text, which are common in domains like healthcare and marketing, thereby limiting its applicability. To address this, we present the Multi-Modal Prior-data Fitted Network (MMPFN), which extends TabPFN to handle tabular and non-tabular modalities in a unified manner. MMPFN comprises per-modality encoders, modality projectors, and pre-trained foundation models. The modality projectors serve as the critical bridge, transforming non-tabular embeddings into tabular-compatible tokens for unified processing. To this end, we introduce a multi-head gated MLP and a cross-attention pooler that extract richer context from non-tabular inputs while mitigates attention imbalance issue in multimodal learning. Extensive experiments on medical and general-purpose multimodal datasets demonstrate that MMPFN consistently outperforms competitive state-of-the-art methods and effectively exploits non-tabular modalities alongside tabular features. These results highlight the promise of extending prior-data fitted networks to the multimodal setting, offering a scalable and effective framework for heterogeneous data learning. The source code is available at <https://github.com/tooz/MultiModalPFN>.

1. Introduction

Tabular data is one of the most widely used data formats across domains such as healthcare, finance, and marketing. Traditionally, gradient-boosted decision trees [7, 14, 35] have dominated this field, owing to their fast training and strong predictive performance. However, recent progress in modern tabular deep learning models [4, 53] has shown that

deep architectures can learn more expressive tabular representations and often surpass traditional tree-based methods.

These advances have also broadened the scope of tabular data analysis to multimodal settings, where structured features are combined with unstructured modalities such as images and text [23]; for example, diagnostic tasks may jointly leverage structured test results and medical images [31, 51], while marketing applications may integrate numerical sales records with textual product reviews [11, 55]. Despite this growing interest, attempts to extend gradient-boosted decision trees to heterogeneous data types have yielded only modest gains, and deep learning models that jointly embed tabular data with images or text, while promising, often suffer from limited performance in data-scarce regimes and slow training [10, 63].

More recently, TabPFN [29, 30] has attracted considerable attention as a tabular foundation model that treats supervised learning on tables as amortized Bayesian inference, achieving strong performance on small- and medium-sized datasets in a single forward pass. While TabPFN establishes a powerful prior over purely tabular distributions, its pretraining is restricted to synthetic tabular data, and no principled extensions to unstructured modalities have been explored. Consequently, despite its strong performance on purely tabular tasks, TabPFN does not address the growing need to jointly model tabular features with image and text modalities in practical multimodal applications.

In this work, we propose the Multi-Modal Prior-data Fitted Network (MMPFN), an extension of TabPFN that processes tabular and non-tabular modalities in a unified manner. MMPFN first extracts features with per-modality encoders for tabular, image, and text inputs. A modality projector then aligns the non-tabular embeddings with the tabular embedding space. The resulting multimodal embeddings are fed into the pretrained TabPFN backbone, so that its tabular prior can be directly reused while incorporating information from images and text through light fine-tuning. In addition, MMPFN explicitly tackles two common failure modes in multimodal learners: overcompressed non-

* Accepted to CVPR 2026.

tabular embeddings and attention imbalance from token-count disparities, by introducing a multi-head gated MLP (MGM) that expands non-tabular representations into multiple tokens and a cross-attention pooler (CAP) that compresses them into a compact, balanced set. MGM and CAP constitute our modality projector. We evaluate MMPFN on multiple benchmarks [1–3, 34, 47, 50] that pair tabular inputs with images or text inputs. Across nearly all datasets, MMPFN surpasses recent state-of-the-art methods [5, 16, 23, 28, 43, 59]. Extensive experiments demonstrate that MGM and CAP effectively mitigate the identified failure modes, while MMPFN scales positively as modalities are added, preserves the strengths of TabPFN’s modeling in low-data regimes. Our main contributions are summarized as follows:

- We propose MMPFN, the first framework to extend TabPFN, pretrained on synthetic tabular distributions, to heterogeneous inputs (tabular + image/text) through a unified pathway.
- We identify two failure modes: overcompressed non-tabular embeddings and token-count-induced attention imbalance, and introduce MGM and CAP as components of the modality projector to address them.
- Through experiments on medical and general-purpose datasets, we show that MMPFN outperforms competitive baselines, scales positively as modalities are added, and maintains robust performance under data scarcity and limited compute.

2. Related works

Vision–Language Multimodal Models Early research in multimodal learning developed fusion and conditioning mechanisms for integrating text and images. FiLM [48] introduced feature-wise modulation for language-conditioned visual reasoning, while early transformer-based models such as ViLBERT, VisualBERT, VL-BERT, LXMERT, and UNITER [8, 37, 42, 54, 57] explored co-attention and unified architectures, achieving state-of-the-art results on vision–language benchmarks. A major shift came with CLIP [49], which used large-scale contrastive pretraining for scalable zero-shot transfer. More recent approaches, such as BLIP-2 [36] and LLaVA [39], integrated large language models for generalizable multimodal reasoning.

Tabular and Multimodal Models The pretraining-driven paradigm has since expanded to structured data. In the tabular domain, approaches typically adopt either a *row-as-text* strategy, serializing entire rows for large language model (LLM) processing [27], or a *per-column embedding* strategy with modality-specific encoders. Methods such as Tab2Text [38] transform rows into textual narratives for improved alignment, while others [5] demonstrate

that careful design of fusion layers substantially improves benchmarks. LANISTR [18] extended this direction with similarity-based multimodal masking, enabling joint learning from language, images, and structured inputs even with missing modalities.

Unstructured–structured integration has also been explored in image-centric datasets. Representative works include MMCL [23], which aligned tabular and image embeddings with contrastive learning; TIP [16], which improved robustness to incomplete features; STiL [17], which leveraged unlabeled data via semi-supervised pseudo-labeling; TIME [43], which employed TabPFN [29] as a tabular encoder; and Turbo [33], which strengthened cross-modal reasoning. Beyond individual models, toolkits such as AutoGluon [58] and modular pipelines [22] provide practical infrastructure for integrating text, image, and tabular features. Despite progress, most multimodal approaches remain concentrated on vision–language tasks, with systematic treatment of structured data still limited. Fusion strategies are often heuristic, with weak guarantees under low-data regimes or modality imbalance. Addressing these gaps is critical for building generalizable multimodal tabular systems.

General-Purpose Pre-trained Models Pretraining large foundation models has transformed representation learning across domains. In NLP, models progressed from masked language modeling to more efficient self-supervised strategies such as ELECTRA [9] and DeBERTa [26]. Later refinements including DeBERTaV3 [25], ModernBERT [61], and multilingual encoders such as BGE/M3 [6] introduced architectural improvements (e.g., disentangled embeddings, FlashAttention-2, optimized tokenization) and broadened applications to retrieval and cross-lingual tasks.

In computer vision, self-supervised pretraining emerged as the dominant paradigm. DINOv2 [45] and DINOv3 [52] demonstrated scalable self-distillation for robust visual features, EVA [19, 20] advanced masked image modeling with large Vision Transformers, and iBOT [64] combined masking with self-distillation for effective ViT representation learning. For structured data, TabPFN [29, 30] extended this paradigm by pretraining on large synthetic datasets, learning a general prior over tabular distributions. This enables strong performance on small- and medium-sized datasets in a single forward pass without task-specific fine-tuning, positioning TabPFN as a foundation model for tabular learning. Taken together, these advances demonstrate the effectiveness of pretraining. Yet, compared to NLP and vision, pretraining for multimodal tabular data remains underexplored. Bridging this gap—particularly for multimodal integration with structured inputs—is a key step toward more comprehensive foundation models.

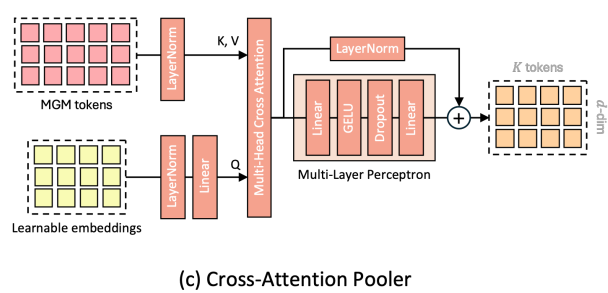
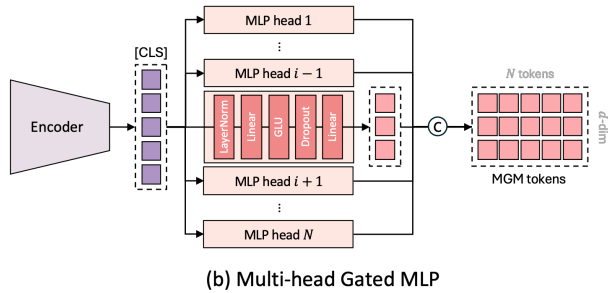
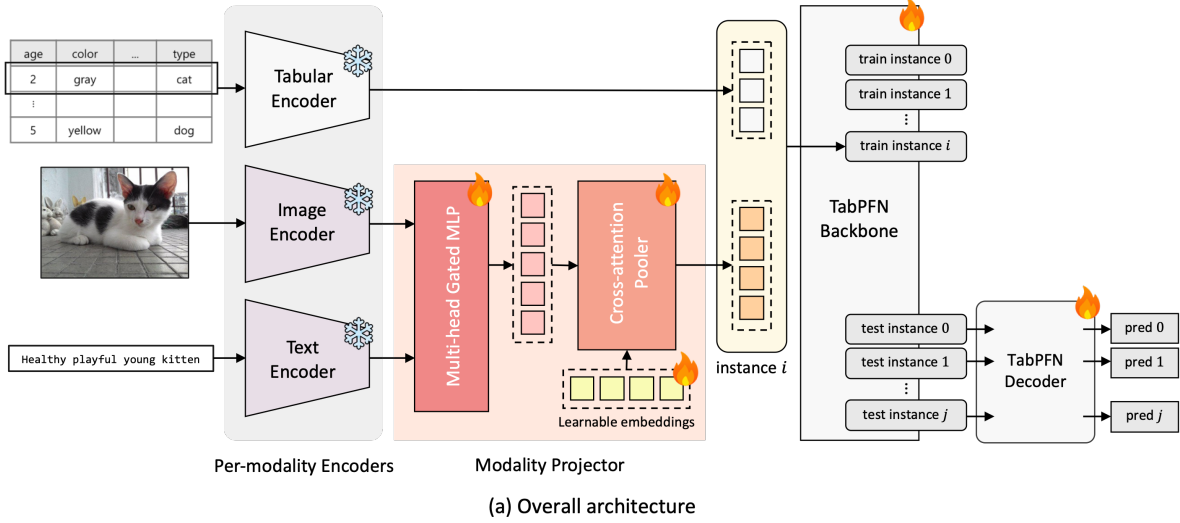


Figure 1. **An overview of MMPFN.** MMPFN extends TabPFN by incorporating per-modality encoders and a modality projector to extract features from non-tabular data. Newly developed components are highlighted in color, while existing ones appear in gray. Layers marked as ‘frozen’ remain fixed during fine-tuning, whereas all others are trainable. Encoded target labels are part of the training inputs but are omitted from the diagram for clarity.

3. Proposed Method

Fig. 1 (a) illustrates the overall architecture of our multi-modal PFN (MMPFN) that extends TabPFN [29, 30] to the multimodal setting, where image or text modalities accompany tabular inputs. Therefore, we begin by briefly reviewing TabPFN. We then describe the proposed multimodal PFN architecture, including the per-modality encoders and the modality projector that aligns non-tabular embeddings with the tabular feature space, followed by the training protocol for fine-tuning MMPFN on downstream multimodal tasks. Finally, we analyze the phenomenon of attention imbalance that arises from token-count disparities across modalities.

3.1. Preliminary: TabPFN

TabPFN [29, 30] is a tabular foundation model that treats tabular learning as amortized Bayesian inference. More specifically, a transformer is pretrained on a large collec-

tion of synthetic tabular datasets sampled from structural causal model priors. During pretraining, it learns to map a small labeled training set and an accompanying query set directly to posterior-predictive label distributions in a single forward pass. Once pretrained, TabPFN can be applied to new tabular tasks without task-specific optimization, simply by feeding the new training–test pairs to the network.

Architecturally, TabPFN stacks 2D TabPFN blocks. Each block splits attention into two stages: feature attention, where each feature attends to other features within the same sample, and sample attention, where the same feature attends across all samples. This design yields permutation invariance over both samples and features and scales efficiently to larger tables than those encountered during pretraining. For in-context inference, TabPFN processes the concatenated training and test rows with masks that allow self-attention within labeled training rows and restrict test rows to cross-attend only to training rows. An MLP head then maps the test embeddings to the predictions.

3.2. Multimodal PFN: Architecture

As shown in Fig. 1 (a), MMPFN consists of per-modality encoders, a modality projector, and a TabPFN backbone. The per-modality encoders map each input modality to a feature representation, while the modality projector aligns image and text embeddings with the shared tabular embedding space. The TabPFN backbone then jointly processes the resulting multimodal embeddings, and a lightweight decoder head produces predictions for the test samples.

Per-Modality Encoders The per-modality encoders comprise tabular, image, and text branches. The tabular branch is identical to the TabPFN v2 encoder [30] and remains frozen during fine-tuning. For images, we employ the DINOv2 ViT-B/14 backbone [15, 46]: input images are resized so that both height and width are divisible by 14, and the final [CLS] token is used as a global image representation. For text, we adopt an ELECTRA-based encoder [9], chosen based on preliminary experiments in which it consistently outperformed DeBERTa variants [24]. Text inputs are tokenized and truncated to a maximum length of 512 tokens, and the corresponding [CLS] embedding is used as the text representation.

Modality Projector The modality projector transforms image and text embeddings into tabular-like representations, which share d -dimensional space compatible with the TabPFN backbone. It comprises two sublayers: a multi-head gated MLP (MGM) and a cross-attention pooler (CAP). MGM addresses the limitation of a single [CLS] embedding, which can overly compress image/text information, by expanding it into N parallel d -dimensional projections. Fig. 1 (b) illustrates the detailed structure of MGM. Specifically, the [CLS] embedding is fed into N MLP heads that project the encoder output dimension to d and produce candidate modality-specific tokens. A Gated Linear Unit (GLU) [12] modulates the contribution of each head, encouraging head-wise specialization and preserving diverse aspects of the original non-tabular representation in the resulting token set.

CAP then balances tabular and non-tabular cues before fusion into the TabPFN backbone. As depicted in Figure 1 (c), it takes the N MGM tokens as keys and values, and introduces K learnable query vectors that attend to them via cross-attention, yielding K representative d -dimensional embeddings per modality. The resulting pooled tokens are further refined by a MLP. These K tokens form a compact and calibrated summary of the image/text information and are concatenated with the tabular tokens along the feature dimension to construct the multimodal input table for TabPFN. Without such pooling, an excessive number of non-tabular tokens can induce attention imbalance,

where the modality with more tokens dominates the attention budget and suppresses tabular signal. CAP mitigates this by producing a compact, calibrated set of embeddings for the TabPFN backbone. We analyze this phenomenon in Section 3.4.

3.3. Multimodal PFN: Training

Since TabPFN is pre-trained on large corpora of synthetic tabular data, its representations can be misaligned with image/text embeddings. We therefore freeze all modality encoders and train the modality projector, the TabPFN backbone, and the decoder. Note that all components are pre-trained, except for the modality projector. To leverage TabPFN’s in-context inference, we follow its standard protocol: split the multimodal data into training and test sets, concatenate their embeddings into a single table, and feed it to the backbone. The model then produces predictions for the test samples to obtain supervisory signals for training.

3.4. Attention Imbalance in MMPFN

We study how the number of non-tabular tokens affects attention mechanism. Consider a query token q attending to two sets of keys: non-tabular tokens $k_1^{(I)}, \dots, k_{N_I}^{(I)}$ and tabular tokens $k_1^{(T)}, \dots, k_{N_T}^{(T)}$, where N_I and N_T are their respective counts. The scaled dot-product attention scores are given by

$$s_i^{(I)} = q^\top k_i^{(I)} / \sqrt{d}, \quad s_j^{(T)} = q^\top k_j^{(T)} / \sqrt{d}. \quad (1)$$

Let $w_i^{(I)} = e^{s_i^{(I)}}$ and $w_j^{(T)} = e^{s_j^{(T)}}$ be the unnormalized attention weights, and define the per-token expectations $c_I = \mathbb{E}[w_i^{(I)}]$ and $c_T = \mathbb{E}[w_j^{(T)}]$, where the expectation is over token indices and any randomness in (q, k) . Also, let a_I denote the total attention weight allocated to the non-tabular set, defined by

$$a_I = \sum_{i=1}^{N_I} \frac{w_i^{(I)}}{\sum_{u=1}^{N_I} w_u^{(I)} + \sum_{v=1}^{N_T} w_v^{(T)}}. \quad (2)$$

Then its expectation is approximated by

$$\mathbb{E}[a_I] \approx \frac{N_I c_I}{N_I c_I + N_T c_T} \quad (3)$$

Hence, when per-token quality is comparable ($c_I \approx c_T$), token-count imbalance ($N_I > N_T$) induces attention imbalance, potentially degrading performance. Consequently, MMPFN’s performance might vary with the modality token ratio. This suggests the importance of CAP. In Section 4, we empirically validate this observation by varying K in the CAP.

Table 1. **Statistics of the multimodal datasets used in our experiments.** “# images” and “# text” denote the number of image and text fields per sample, respectively. PetFinder variants indicate which modalities (tabular (T), image (I), text (t)) are used.

Dataset	# train samples	# test samples	# features	# numeric features	# categorical features	# images	# text	# classes
PAD-UFES-20 [47]	1838	460	21	3	18	1	0	6
CBIS-DDSM(Mass) [50]	1318	378	8	3	5	3	0	2
CBIS-DDSM(Calc) [50]	1546	326	8	3	5	3	0	2
Airbnb [1]	5465	1367	50	27	23	0	1	10
Salary [3]	15841	3961	4	1	3	0	3	6
Cloth [2]	18788	4698	5	2	3	0	3	5
PetFinder-I (T+I) [34]	11721	2931	19	5	14	1	0	5
PetFinder-t (T+t) [34]	11721	2931	19	5	14	0	1	5
PetFinder-A (T+I+t) [34]	11721	2931	19	5	14	1	1	5

4. Experiments

4.1. Experimental Setup

Dataset. We evaluate MMPFN using well-established multimodal datasets that have been extensively validated in previous studies [5, 32, 44, 58, 59]:

- PAD-UFES-20(PU20) [47] contains 2,298 samples from six skin lesion types, each paired with a clinical image and up to 26 metadata features.
- CBIS-DDSM [50] is a curated subset of the DDSM containing digitized mammography images with annotated regions of interest for calcifications and masses, biopsy-verified benign/malignant labels, and rich lesion-level metadata.
- Airbnb [1] provides a detailed snapshot of Melbourne’s homestay activity as of December 2018; following the preprocessing strategy of TTT, we discretize the target into ten quantile-based groups of equal size.
- Salary [3] contains 15,841 training and 3,961 test job postings from India, each with company, years of experience, job description, designation, job type, key skills, and location, with the task of predicting the salary range.
- Cloth [2] comprises 23,486 customer reviews with textual fields and 10 tabular features, providing a multimodal benchmark for sentiment and recommendation prediction.
- PetFinder [34], released for the Kaggle PetFinder.my challenge, contains over 14,000 pet profiles with images, descriptive text, and structured attributes for predicting a five-class adoption-speed outcome.

For each dataset, we randomly split the data into training and test sets, except for CBIS-DDSM, for which we use the predefined train-test split. Table 1 summarizes the statistics of these datasets. More details about datasets are provided in the supplementary material.

Implementation Details. We fine-tune MMPFN for 100 iterations to minimize the cross-entropy loss. We employ AdamW [41] with learning rate of 1×10^{-5} and batch

Table 2. **Comparison with state-of-the-arts on image-tabular multimodal datasets.** Performance is reported as “accuracy (rank)”, where the accuracy are averaged over five random seeds and the rank represents the ordering of the methods according to their accuracy within each dataset (lower rank indicates better performance). “Avg.” denote the averaged accuracy across datasets. Best accuracy is shown in **bold**, second best in underline.

Method	PU20	Mass	Calc	Petfinder	Avg.
TabPFN [29]	82.17 (2)	71.27 (5)	73.31 (2)	36.33 (8)	4.25
Catboost [14]	80.43 (4)	78.31 (1)	72.09 (4)	38.69 (4)	<u>3.25</u>
AutoGluon [58]	81.09 (3)	<u>76.28 (2)</u>	71.04 (6)	38.81 (3)	3.50
MMCL [23]	76.61 (7)	<u>57.62 (7)</u>	60.12 (8)	36.61 (7)	7.25
TIP [16]	78.75 (6)	73.12 (4)	67.96 (7)	37.28 (5)	5.50
HEALNet [28]	74.65 (8)	68.10 (6)	71.83 (5)	37.03 (6)	6.25
TIME [43]	80.35 (5)	-	72.70 (3) ¹	<u>39.25 (2)</u>	3.33
MMPFN	85.22 (1)	74.53 (3)	75.40 (1)	40.74 (1)	1.50

size of 1. For all experiments, random seeds are fixed to $\{0, 1, 2, 3, 4\}$ and then report the averaged accuracy to assess the performance of the proposed method. More implementation details are provided in the supplementary material.

4.2. Main Results

Results on Tabular–Image Modality Datasets. Table 2 summarizes the classification accuracy of MMPFN and state-of-the-art baselines on four tabular–image datasets. Compared with fine-tuned TabPFN [30], which use only tabular inputs, MMPFN consistently improves performance by leveraging image features. In Table 2, MMCL [23], TIP [16], and HEALNet [28] show inconsistent performance, due to small dataset size and the low dimensionality of tabular features. In contrast, MMPFN achieves the best

¹We cite all results of Luo et al. [43] directly. Although TIME used the CBIS-DDSM dataset without specifying subtype, the reported sample size matches the calcification subset, so we list it under CBIS-DDSM calcification in Table 2. Since the code is unavailable, reproduction was infeasible.

results on all datasets except Mass, where its performance is only marginally different from the other two models. Compared with TIME [43], which uses TabPFN as its tabular encoder, MMPFN delivers substantial gains, indicating that our modality projection strategies are more effective than simple fusion. CatBoost [14] incorporated image embeddings as raw input features, following the recommendations in its documentation, and achieved strong performance. AutoGluon [58], an AutoML framework for multimodal data, also performed competitively on several tabular benchmarks. However, both models exhibited a lower average rank than MMPFN.

Results on Tabular–Text Modality Datasets. Table 3 reports results on tabular–text modality datasets. As in the image setting, adding text features consistently outperforms the fine-tuned TabPFN baseline. MMPFN is particularly strong on Airbnb. This dataset includes 50+ tabular features and a single text field, allowing tabular-specialized models to capture most of the predictive signal. Accordingly, MMPFN substantially outperforms language model–based methods, such as TFN [62] and MulT [60], which struggle to exploit the abundant tabular features. By contrast, in Cloth, the tabular part has few, weakly informative features, while the review text carries most of the signal. This is reflected in the poor performance of tabular-only models and the strong results of AllTextBERT [5], indicating that text-specialized models excel in such cases. Even so, among methods that explicitly preserve tabular structure, MMPFN achieves the best overall performance, trailing the text-specialized baseline by only a small margin. This contrasts with prior multimodal tabular studies, which emphasized tabular-dominant datasets [23]. Overall, MMPFN is not merely strong on tabular inputs. It also models unstructured modalities effectively, establishing it as a truly multimodal approach.

4.3. Analysis

MMPFN as an Image and Text Classifier, Fig. 2a evaluates MMPFN with non-tabular-only inputs. For the baseline, we extract the pre-trained DINOv2 [45] or Electra [9] [CLS] embedding and train an attached MLP head for classification—an approach that is widely adopted and often near-optimal [56]. MMPFN generated non-tabular feature embeddings from the CLS token using only MGM. With non-tabular embeddings as the sole inputs, MMPFN is within ~1% of DINOv2 (69.30% vs. 69.89%). Accuracy increases consistently as the number of image feature tokens grows, indicating that additional tokens capture com-

¹AllTextBert converts all tabular features into strings, concatenates them, and inputs the resulting sequence into DistilBERT–base–uncased for modeling, as described in [5].

Table 3. **Comparison with state-of-the-arts on text-tabular multimodal datasets.** Performance is reported as “accuracy (rank)”, where the accuracy are averaged over five random seeds and the rank represents the ordering of the methods according to their accuracy within each dataset (lower rank indicates better performance). “Avg.” denote the averaged accuracy across datasets. Best accuracy is shown in **bold**, second best in underline.

Method	Airbnb	Salary	Cloth	Petfinder	Avg.
TabPFN [29]	<u>46.96 (2)</u>	44.96 (6)	55.07 (8)	36.33 (6)	5.50
Catboost [14]	43.56 (4)	40.36 (8)	59.24 (7)	35.47 (7)	6.50
AutoGluon [58]	44.60 (3)	45.24 (5)	72.07(1)	37.96 (3)	<u>3.00</u>
AllTextBERT [5]	30.9 (8)	44.0 (7)	<u>68.0(2)</u>	34.6 (8)	6.25
TFN [62]	35.7 (7)	45.8 (3)	60.1 (6)	36.8 (5)	5.25
MulT [60]	36.3 (6)	45.4 (4)	63.6 (5)	37.6 (4)	4.75
TTT [5]	38.3 (5)	47.2 (1)	65.5 (4)	<u>38.9 (2)</u>	<u>3.00</u>
MMPFN	47.78 (1)	<u>46.17 (2)</u>	66.26 (3)	39.04 (1)	1.75

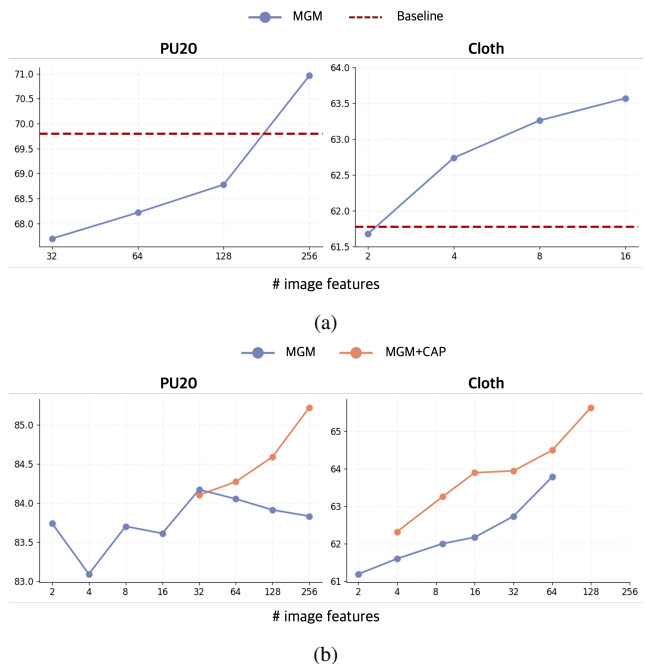


Figure 2. **Performance on PU20 and Cloth as a function of the number of non-tabular features.** (a) Results from non-tabular-only experiments using DINOv2/ELECTRA with an MLP baseline. (b) Results from multi-modal token imbalance experiments. In both settings, the y-axis denotes accuracy, while the x-axis corresponds to the number of non-tabular input features. For (b), when applying MGM+CAP, the number of CAP heads was fixed at 24 and 4, respectively.

plementary, higher-resolution information. Thus, despite being trained with a tabular synthetic data, MMPFN functions effectively as a classifier over image embeddings cast into tabular-like features, highlighting seamless integration

Table 4. **Ablation on the modality projector design.** We compare single-head and multi-head feature extraction mechanisms (Linear/MLP, MoE, and the proposed MGM) across all datasets. MoE denotes Mixture-of-Experts. Best results are highlighted in **bold**.

Category	Method	PU20	Mass	Calc	Cloth	Salary	Airbnb	PetFinder-I	PetFinder-T	PetFinder-A	Avg.
Single-head	Linear	83.48	66.19	74.17	58.06	44.67	47.02	37.22	36.64	37.30	53.86
	MLP	83.78	64.87	73.87	60.44	44.33	46.85	37.22	36.64	37.30	54.14
Multi-head	MLP	84.39	67.99	73.99	64.39	45.93	46.79	40.64	38.12	40.04	55.81
	MoE	83.22	66.67	73.13	55.07	44.25	46.12	36.82	36.83	36.94	53.23
	MGM	85.22	74.53	75.40	66.26	46.17	47.78	40.70	39.04	41.19	57.37

of non-tabular modalities with tabular data. We also note that the presence of CAP yields a modest additional gain for MMPFN.

Attention Imbalance. We empirically investigate attention imbalance in multimodal processing. Fig. 2a shows the performance of MMPFN when only non-tabular features are provided as input. We use PU as the image dataset and Cloth as the text dataset. The results show that performance increases as the number of MGM heads increases, indicating that performance improves for both image and text modalities as the number of extracted non-tabular features grows. In this setting, CAP is not used to consolidate inputs. From these results, we confirm that a PFN trained solely on synthetic tabular data can classify image and text features—once projected into a tabular feature space—with performance comparable to or better than general baselines. This suggests that TabPFN has the potential to operate not only as a tabular-specific model but also as a model capable of handling multiple modalities.

However, as shown in Fig. 2b, when tabular and non-tabular features are provided together as input, naively increasing the number of non-tabular features can degrade performance. MMPFN achieves its highest accuracy when the counts of tabular and non-tabular features are similar, and performance declines as one modality dominates the token composition. This contrasts with Fig. 2a, where MMPFN operates in a non-tabular-only setting and does not exhibit a performance drop as the number of non-tabular features increases. This non-monotonic pattern is consistent with attention imbalance: when one modality occupies most of the input tokens, it absorbs a disproportionately large share of the attention budget. Tokens from the minority modality receive relatively little attention, diluting their useful signals, while noise features from the majority modality may still receive nonzero attention, ultimately degrading performance.

The proposed MGM+CAP mitigates this issue by first extracting non-tabular features using a sufficient number of MGM heads and then consolidating them. As a result, MGM+CAP improves steadily as the number of MGM

heads increases and outperforms the MGM-only setup. The MGM head count corresponds to the x-axis, and CAP converts the extracted features into a compact, fixed-size representation—24 tokens for PU20 and 4 tokens for Cloth, preserving essential information while capping the overall token count. More detailed experimental results related to attention imbalance are provided in the supplementary material.

Modality Projector. Table 4 summarizes an ablation of the modality projector design, comparing single-head (Linear, MLP) and multi-head (MLP, MoE, MGM) variants across all datasets. Single-head baselines, which apply a single linear or MLP projection to the non-tabular [CLS] embedding, already improve over the tabular-only backbone but yield the lowest average accuracies, highlighting the limitation of overcompressed representations.

Moving to a multi-head projector that expands [CLS] into multiple tokens consistently boosts performance, confirming the benefit of capturing diverse aspects of the image/text features. Within the multi-head family, the Mixture-of-Experts (MoE) variant is less effective and less stable across datasets, suggesting that sparse expert routing is hard to exploit in the low-data regime considered here. In contrast, the proposed MGM, which combines multi-head projection with GLU-based gating, achieves the best accuracy on every dataset and the highest overall average.

Correlation Analysis of Cross-Modal Embeddings

Fig. 3 visualizes cosine similarities among TabPFN-backbone embeddings on all tabular-image and tabular-text datasets. These similarities illustrate the predictive relationships between features learned by MMPFN. As expected, within-modality blocks exhibit high similarity. However, several tabular-image/text pairs are also strongly aligned, indicating that MMPFN models cross-modal interactions rather than only within-modality structure. Details of the cosine similarity computation are provided in supplementary material.

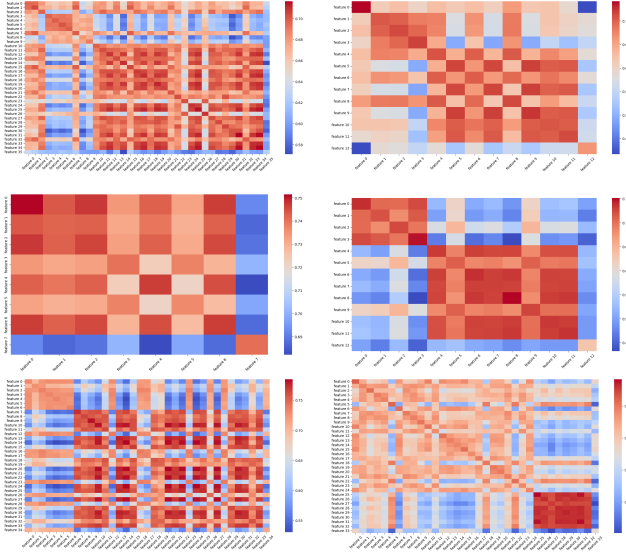


Figure 3. **Cosine similarity between multimodal feature embeddings.** Axes denote all tabular and text/image features. From left to right and top to bottom, it shows the correlations between features in the experiments on the PU20, Calc, Cloth, Mass, Petfinder, and Airbnb datasets.

Table 5. **Performance in Low-data Regime.** Each method uses two rows: accuracy (top) and percentage change vs. full-data (bottom). The ‘Avg.’ column averages percentage changes only. Best accuracy is in **bold**.

	PU20	Mass	Calc	PetFinder	Avg.
TIP [16] 10%	70.44 (-10.6)	68.31 (-6.58)	62.27 (-8.37)	34.86 (-6.49)	58.97 -8.00
MMPFN 10%	72.87 (-14.14)	76.13 (+0.75)	72.09 (-5.23)	35.73 (-12.30)	64.21 -10.27

Robustness in Low-Data Regimes Tabular datasets often require expert annotation, resulting in limited sample sizes and sparse labels [16, 17]. Consequently, models that remain robust under data scarcity are highly desirable. In such low-data regimes, MMPFN demonstrates strong performance. Table 5 compares the results of MMPFN and TIP when trained on only 10% of randomly selected samples from each dataset. While TIP employs self-supervised pretraining using all unlabeled data, our evaluation focuses on supervised finetuning under limited labeled data.

The analysis shows that, although the relative performance drop was larger for MMPFN, it consistently outperformed TIP across all datasets, even when trained with only 10% of the data. Interestingly, on the CBIS-DDSM Mass dataset, performance improved under subsampling. This behavior suggests that the PFN, pretrained on synthetic pri-

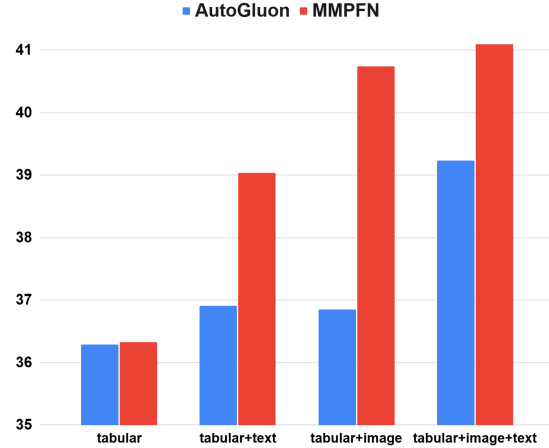


Figure 4. **Accuracy of AutoGluon vs. MMPFN on PetFinder** under different modality combinations: tabular, +text, +image, +image+text.

ors, can better capture discriminative characteristics when finetuned on a smaller set of labeled examples. Additional details on the behavior of MMPFN in low-data settings are provided in the supplementary material.

Scaling with Added Modalities We assess MMPFN as multiple non-tabular modalities are added. On Petfinder, we compare against AutoGluon, a multimodal AutoML system supporting image and text modalities. As shown in Fig. 4, MMPFN’s accuracy increases monotonically from *tabular* → *tabular+text* → *tabular+image* → *tabular+image+text* (39% → 40% → 41%), indicating complementary signal from both image and text. These results have particular significance for tabular modeling, where performance improvements from architectural changes alone are often saturated. Adding complementary modalities offers a practical route to further gains. Moreover, MMPFN outperforms AutoGluon under every combination. Unlike AutoGluon’s large ensembles, MMPFN achieves higher accuracy with a lightweight and specialized architecture.

5. Conclusion

We introduced MMPFN, a multimodal extension of TabPFN that unifies tabular, image, and text inputs with per-modality encoders, a modality projector, and the TabPFN backbone. We developed MGM and CAS, which map non-tabular embeddings to the tabular space and mitigate token-count-induced attention imbalance. By leveraging pretrained foundation models and finetuning lightweight components, MMPFN achieved strong accuracy with substantially lower training costs. Across medical and general-purpose benchmarks, it consistently outperformed competitive state-of-the-art

methods, scaled positively as modalities were added, and maintained robust performance in low-data regimes.

References

- [1] kaggle.com/datasets/tylerx/melbourne-airbnb-open-data. 2, 5
- [2] kaggle.com/datasets/nicapotato/womens-ecommerce-clothing-reviews. 5
- [3] kaggle.com/datasets/anitkalauni/predict-the-data-scientists-salary-in-india. 2, 5
- [4] Dara Bahri, Heinrich Jiang, Yi Tay, and Donald Metzler. Scarf: Self-supervised contrastive learning using random feature corruption. *arXiv preprint arXiv:2106.15147*, 2021. 1
- [5] Thomas Bonnier. Revisiting multimodal transformers for tabular data with text fields. In *Findings of the Association for Computational Linguistics: ACL 2024*, pages 1481–1500, 2024. 2, 5, 6, 3
- [6] Jianlv Chen, Shitao Xiao, Peitian Zhang, Kun Luo, Defu Lian, and Zheng Liu. Bge m3-embedding: Multilingual, multi-functionality, multi-granularity text embeddings through self-knowledge distillation. *arXiv preprint arXiv:2309.07597*, 2023. 2
- [7] Tianqi Chen and Carlos Guestrin. Xgboost: A scalable tree boosting system. In *Proceedings of the 22nd acm sigkdd international conference on knowledge discovery and data mining*, pages 785–794, 2016. 1
- [8] Yen-Chun Chen, Linjie Li, Licheng Yu, Ahmed El Kholy, Faisal Ahmed, Zhe Gan, Yu Cheng, and Jingjing Liu. Uniter: Universal image-text representation learning. In *ECCV*, pages 104–120. Springer, 2020. 2
- [9] Kevin Clark, Minh-Thang Luong, Quoc V. Le, and Christopher D. Manning. ELECTRA: Pre-training text encoders as discriminators rather than generators. In *ICLR*, 2020. 2, 4, 6
- [10] Can Cui, Haichun Yang, Yaohong Wang, Shilin Zhao, Zuhayr Asad, Lori A Coburn, Keith T Wilson, Bennett A Landman, and Yuankai Huo. Deep multimodal fusion of image and non-image data in disease diagnosis and prognosis: a review. *Progress in Biomedical Engineering*, 5(2):022001, 2023. 1
- [11] Ronnie Das, Wasim Ahmed, Kshitij Sharma, Mariann Hardey, Yogesh K Dwivedi, Ziqi Zhang, Chrysostomos Apostolidis, and Raffaele Filieri. Towards the development of an explainable e-commerce fake review index: An attribute analytics approach. *European Journal of Operational Research*, 317(2):382–400, 2024. 1
- [12] Yann N Dauphin, Angela Fan, Michael Auli, and David Grangier. Language modeling with gated convolutional networks. In *International Conference on Machine Learning (ICML)*, pages 933–941. PMLR, 2017. 4
- [13] Aaron Defazio, Xingyu Yang, Ahmed Khaled, Konstantin Mishchenko, Harsh Mehta, and Ashok Cutkosky. The road less scheduled. In *Adv. Neural Inform. Process. Syst.*, pages 9974–10007, 2024. 3
- [14] Anna Veronika Dorogush, Vasily Ershov, and Andrey Gulin. Catboost: gradient boosting with categorical features support. *arXiv preprint arXiv:1810.11363*, 2018. 1, 5, 6
- [15] Alexey Dosovitskiy. An image is worth 16x16 words: Transformers for image recognition at scale. In *ICLR*, 2021. 4
- [16] Siyi Du, Shaoming Zheng, Yinsong Wang, Wenjia Bai, Declan P O’Regan, and Chen Qin. Tip: Tabular-image pre-training for multimodal classification with incomplete data. In *ECCV*, pages 478–496. Springer, 2024. 2, 5, 8, 3
- [17] Siyi Du, Xinzhe Luo, Declan P O’Regan, and Chen Qin. Stil: Semi-supervised tabular-image learning for comprehensive task-relevant information exploration in multimodal classification. In *CVPR*, pages 15549–15559, 2025. 2, 8, 3
- [18] Sayna Ebrahimi, Serkan O Arik, Yihe Dong, and Tomas Pfister. Lanistr: Multimodal learning from structured and unstructured data. *arXiv preprint arXiv:2305.16556*, 2023. 2
- [19] Yuxin Fang, Wen Wang, Binhui Xie, Quan Sun, Ledell Wu, Xinggong Wang, Tiejun Huang, Xinlong Wang, and Yue Cao. Eva: Exploring the limits of masked visual representation learning at scale. *arXiv preprint arXiv:2211.07636*, 2022. 2
- [20] Yuxin Fang, Quan Sun, Xinggong Wang, Tiejun Huang, Xinlong Wang, and Yue Cao. Eva-02: A visual representation for neon genesis. *Image and Vision Computing*, 149:105171, 2024. 2
- [21] Arthur Gretton, Karsten M Borgwardt, Malte J Rasch, Bernhard Schölkopf, and Alexander Smola. A kernel two-sample test. *The journal of machine learning research*, 13(1):723–773, 2012. 1
- [22] Ken Gu and Akshay Budhkar. A package for learning on tabular and text data with transformers. In *Proceedings of the Third Workshop on Multimodal Artificial Intelligence*, pages 69–73, 2021. 2
- [23] Paul Hager, Martin J Menten, and Daniel Rueckert. Best of both worlds: Multimodal contrastive learning with tabular and imaging data. In *CVPR*, pages 23924–23935, 2023. 1, 2, 5, 6, 3
- [24] Pengcheng He, Xiaodong Liu, Jianfeng Gao, and Weizhu Chen. Deberta: Decoding-enhanced bert with disentangled attention. In *ICLR*, 2020. 4
- [25] Pengcheng He, Jianfeng Gao, and Weizhu Chen. Debertav3: Improving deberta using electra-style pre-training with gradient-disentangled embedding sharing. *arXiv preprint arXiv:2111.09543*, 2021. 2
- [26] Pengcheng He, Xiaodong Liu, Jianfeng Gao, and Weizhu Chen. Deberta: Decoding-enhanced bert with disentangled attention. In *ICLR*, 2021. 2
- [27] Stefan Hegselmann, Alejandro Buendia, Hunter Lang, Monica Agrawal, Xiaoyi Jiang, and David Sontag. Tabllm: Few-shot classification of tabular data with large language models. In *International conference on artificial intelligence and statistics*, pages 5549–5581. PMLR, 2023. 2
- [28] Konstantin Hemker, Nikola Simidjievski, and Mateja Jamnik. Healnet: Multimodal fusion for heterogeneous biomedical data. *arXiv preprint arXiv:2311.09115*, 2024. 2, 5
- [29] Noah Hollmann, Samuel Müller, Katharina Eggenberger, and Frank Hutter. TabPFN: A transformer that solves small

- tabular classification problems in a second. In *ICLR*, 2022. 1, 2, 3, 5, 6
- [30] Noah Hollmann, Samuel Müller, Lennart Purucker, Arjun Krishnakumar, Max Körfer, Shi Bin Hoo, Robin Tibor Schirrmeyer, and Frank Hutter. Accurate predictions on small data with a tabular foundation model. *Nature*, 637(8045):319–326, 2025. 1, 2, 3, 4, 5
- [31] Shih-Cheng Huang, Anuj Pareek, Saeed Seyyedi, Imon Banerjee, and Matthew P Lungren. Fusion of medical imaging and electronic health records using deep learning: a systematic review and implementation guidelines. *NPJ digital medicine*, 3(1):136, 2020. 1
- [32] Jun-Peng Jiang, Han-Jia Ye, Leye Wang, Yang Yang, Yuan Jiang, and De-Chuan Zhan. Tabular insights, visual impacts: transferring expertise from tables to images. In *Forty-first International Conference on Machine Learning (ICML)*, 2024. 5
- [33] Jun-Peng Jiang, Yu Xia, Hai-Long Sun, Shiyin Lu, Qing-Guo Chen, Weihua Luo, Kaifu Zhang, De-Chuan Zhan, and Han-Jia Ye. Multimodal tabular reasoning with privileged structured information. *arXiv preprint arXiv:2506.04088*, 2025. 2
- [34] Kaggle. Petfinder.my adoption prediction. <https://www.kaggle.com/competitions/petfinder-adoption-prediction>, 2019. Accessed: September 24, 2025. 2, 5
- [35] Guolin Ke, Qi Meng, Thomas Finley, Taifeng Wang, Wei Chen, Weidong Ma, Qiwei Ye, and Tie-Yan Liu. Lightgbm: A highly efficient gradient boosting decision tree. In *Adv. Neural Inform. Process. Syst.*, 2017. 1
- [36] Junnan Li, Dongxu Li, Silvio Savarese, and Steven Hoi. Blip-2: Bootstrapping language-image pre-training with frozen image encoders and large language models. In *International Conference on Machine Learning (ICML)*, pages 19730–19742. PMLR, 2023. 2
- [37] Liunian Harold Li, Mark Yatskar, Da Yin, Cho-Jui Hsieh, and Kai-Wei Chang. Visualbert: A simple and performant baseline for vision and language. *arXiv preprint arXiv:1908.03557*, 2019. 2
- [38] Tong Lin, Jason Yan, David Jurgens, and Sabina J Tomkins. Tab2Text - a framework for deep learning with tabular data. In *Findings of the Association for Computational Linguistics: EMNLP 2024*, pages 12925–12935, 2024. 2
- [39] Haotian Liu, Chunyuan Li, Qingyang Wu, and Yong Jae Lee. Visual instruction tuning. In *Adv. Neural Inform. Process. Syst.*, pages 34892–34916, 2023. 2
- [40] Mingsheng Long, Han Zhu, Jianmin Wang, and Michael I Jordan. Deep transfer learning with joint adaptation networks. In *International Conference on Machine Learning (ICML)*, pages 2208–2217. PMLR, 2017. 1
- [41] Ilya Loshchilov and Frank Hutter. Decoupled weight decay regularization. In *ICLR*, 2019. 5
- [42] Jiasen Lu, Dhruv Batra, Devi Parikh, and Stefan Lee. Vilbert: Pretraining task-agnostic visiolinguistic representations for vision-and-language tasks. In *Adv. Neural Inform. Process. Syst.*, 2019. 2
- [43] Jiaqi Luo, Yuan Yuan, and Shixin Xu. Time: TabPFN-integrated multimodal engine for robust tabular-image learning. *arXiv preprint arXiv:2506.00813*, 2025. 2, 5, 6
- [44] Martin Mráz, Breenda Das, Anshul Gupta, Lennart Purucker, and Frank Hutter. Towards benchmarking foundation models for tabular data with text. *arXiv preprint arXiv:2507.07829*, 2025. 5
- [45] Maxime Oquab, Timothée Darcet, Théo Moutakanni, Huy Vo, Marc Szafraniec, Vasil Khalidov, Pierre Fernandez, Daniel Haziza, Francisco Massa, Alaaeldin El-Nouby, et al. Dinov2: Learning robust visual features without supervision. *arXiv preprint arXiv:2304.07193*, 2023. 2, 6
- [46] Maxime Oquab, Timothée Darcet, Théo Moutakanni, Huy V Vo, Marc Szafraniec, Vasil Khalidov, Pierre Fernandez, Daniel HAZIZA, Francisco Massa, Alaaeldin El-Nouby, et al. Dinov2: Learning robust visual features without supervision. *Trans. Mach. Learn. Res.*, 1, 2024. 4
- [47] Andre GC Pacheco, Gustavo R Lima, Amanda S Salomao, Breno Krohling, Igor P Biral, Gabriel G De Angelo, Fábio CR Alves Jr, José GM Esgario, Alana C Simora, Pedro BC Castro, et al. Pad-ufes-20: A skin lesion dataset composed of patient data and clinical images collected from smartphones. *Data in Brief*, 32:106221, 2020. 2, 5
- [48] Ethan Perez, Florian Strub, Harm De Vries, Vincent Dumoulin, and Aaron Courville. Film: Visual reasoning with a general conditioning layer. In *AAAI*, 2018. 2
- [49] Alec Radford, Jong Wook Kim, Chris Hallacy, Aditya Ramesh, Gabriel Goh, Sandhini Agarwal, Girish Sastry, Amanda Askell, Pamela Mishkin, Jack Clark, et al. Learning transferable visual models from natural language supervision. In *International Conference on Machine Learning (ICML)*, pages 8748–8763. PMLR, 2021. 2
- [50] Rebecca Sawyer-Lee, Francisco Gimenez, Assaf Hoogi, and Daniel Rubin. Curated breast imaging subset of digital database for screening mammography (cbis-ddsm). (*No Title*), 2016. 2, 5
- [51] Jörg Schilcher, Alva Nilsson, Oliver Andlid, and Anders Eklund. Fusion of electronic health records and radiographic images for a multimodal deep learning prediction model of atypical femur fractures. *Computers in Biology and Medicine*, 168:107704, 2024. 1
- [52] Oriane Siméoni, Huy V Vo, Maximilian Seitzer, Federico Baldassarre, Maxime Oquab, Cijo Jose, Vasil Khalidov, Marc Szafraniec, Seungeun Yi, Michaël Ramamonjisoa, et al. Dinov3. *arXiv preprint arXiv:2508.10104*, 2025. 2
- [53] Gowthami Somepalli, Micah Goldblum, Avi Schwarzschild, C Bayan Bruss, and Tom Goldstein. Saint: Improved neural networks for tabular data via row attention and contrastive pre-training. *arXiv preprint arXiv:2106.01342*, 2021. 1
- [54] Weijie Su, Xizhou Zhu, Yue Cao, Bin Li, Lewei Lu, Furu Wei, and Jifeng Dai. ViLbert: Pre-training of generic visiolinguistic representations. *arXiv preprint arXiv:1908.08530*, 2019. 2
- [55] Maarten Sukel, Stevan Rudinac, and Marcel Worring. Multimodal temporal fusion transformers are good product demand forecasters. *IEEE MultiMedia*, 31(2):48–60, 2024. 1

- [56] Chi Sun, Xipeng Qiu, Yige Xu, and Xuanjing Huang. How to fine-tune bert for text classification? In *China national conference on Chinese computational linguistics*, pages 194–206. Springer, 2019. [6](#)
- [57] Hao Tan and Mohit Bansal. Lxmert: Learning cross-modality encoder representations from transformers. *arXiv preprint arXiv:1908.07490*, 2019. [2](#)
- [58] Zhiqiang Tang, Haoyang Fang, Su Zhou, Taojiannan Yang, Zihan Zhong, Tony Hu, Katrin Kirchhoff, and George Karypis. Autogluon-multimodal (automm): Supercharging multimodal automm with foundation models. *arXiv preprint arXiv:2404.16233*, 2024. [2](#), [5](#), [6](#)
- [59] Zhiqiang Tang, Zihan Zhong, Tong He, and Gerald Friedland. Bag of tricks for multimodal automm with image, text, and tabular data. *arXiv preprint arXiv:2412.16243*, 2024. [2](#), [5](#)
- [60] Yao-Hung Hubert Tsai, Shaojie Bai, Paul Pu Liang, J. Zico Kolter, Louis-Philippe Morency, and Ruslan Salakhutdinov. Multimodal transformer for unaligned multimodal language sequences. In *Proceedings of the 57th Annual Meeting of the Association for Computational Linguistics*, pages 6558–6569, 2019. [6](#)
- [61] Benjamin Warner, Antoine Chaffin, Benjamin Clavié, Orion Weller, Oskar Hallström, Said Taghadouini, Alexis Gallagher, Raja Biswas, Faisal Ladhak, Tom Aarsen, Nathan Cooper, Griffin Adams, Jeremy Howard, and Iacopo Poli. Smarter, better, faster, longer: A modern bidirectional encoder for fast, memory efficient, and long context finetuning and inference. *arXiv preprint arXiv:2412.13663*, 2024. [2](#)
- [62] Amir Zadeh, Minghai Chen, Soujanya Poria, Erik Cambria, and Louis-Philippe Morency. Tensor fusion network for multimodal sentiment analysis. In *Proceedings of the 2017 Conference on Empirical Methods in Natural Language Processing (EMNLP)*, pages 1103–1114, 2017. [6](#)
- [63] Fei Zhao, Chengcui Zhang, and Baocheng Geng. Deep multimodal data fusion. *ACM computing surveys*, 56(9):1–36, 2024. [1](#)
- [64] Jinghao Zhou, Chen Wei, Huiyu Wang, Wei Shen, Cihang Xie, Alan Yuille, and Tao Kong. ibot: Image bert pre-training with online tokenizer. In *ICLR*, 2022. [2](#)
- [65] Xuran Zhu. Cross-modal domain adaptation in brain disease diagnosis: Maximum mean discrepancy-based convolutional neural networks. In *2024 6th International Conference on Communications, Information System and Computer Engineering (CISCE)*, pages 1515–1519. IEEE, 2024. [1](#)

MultiModalPFN: Extending Prior-Data Fitted Networks for Multimodal Tabular Learning

Accepted to CVPR 2026.

Supplementary Material

S1. Additional Analysis

Attention Imbalance. Fig. S1 illustrates the relationship between the number of non-tabular input features generated by MGM and CAP and the resulting performance across the evaluated datasets. In all cases, the best performance is achieved when the number of non-tabular features is similar to the number of tabular features. Performance tends to degrade when the number of non-tabular features is either substantially smaller or larger than the number of tabular features. These results experimentally support our analysis of attention imbalance.

Activation Choice in MGM. We study the impact of using GLU as the activation function in MGM on the CBIS-DDSM (MASS) and Salary datasets. Table S1 compares GLU against a GELU baseline in terms of accuracy and mean output-vector orthogonality. Since GLU reduces the dimensionality by half after the gating operation, the GELU baseline is configured with more parameters. Despite this advantage, GLU consistently yields higher accuracy than GELU on both datasets, while also increasing the orthogonality measure. This suggests that the gating mechanism in GLU not only improves predictive performance but also promotes more diverse output representations, aligning with our objective of learning complementary non-tabular features. Consequently, we adopt GLU as the default activation in MGM.

Table S1. **Effect of activation choice in MGM.** Comparison of accuracy and mean output-vector orthogonality when using GELU versus GLU, with and without orthogonality loss, on CBIS-DDSM (MASS) and Salary.

Activation	CBIS-DDSM (MASS)		Salary	
	Accuracy	Orthogonality	Accuracy	Orthogonality
GELU	72.09	0.0565	45.04	0.04876
GLU	75.10	0.0913	45.87	0.05831

Robustness of Low-Data Regimes. In Table 5, MMPFN achieves a higher average performance (64.21) than TIP (58.97), despite larger relative drops on PU20 and Petfinder. This robustness primarily stems from strong priors learned during large-scale meta-training on synthetic datasets [29, 30], which capture a broad range of plausible tabular distributions and enable effective generalization from few real

samples. Fine-tuning then provides a light task-specific adaptation on top of this Bayesian inference. Because the model requires only light adaptation, it avoids overfitting and remains stable in low-sample settings. Together with the inductive bias of the Per-Feature Transformer, this explains the superior performance of our MMPFN across low-data experiments.

Replacing Modality Encoder MMPFN combines pre-trained models, making the framework naturally extensible as newer and stronger encoders become available. This modular design allows components such as TabPFN or DINO to be replaced with more recent architectures without altering the overall pipeline. Leveraging improved pre-trained models enhances the quality of feature representations and can lead to measurable downstream gains. For example, substituting DINOv2 with the recently released DINOv3 yields consistent improvements across datasets, as shown in Section S1; on PU20, accuracy increases by approximately 0.74 percentage points.

Table S2. **Effect of replacing the image encoder.** Performance of MMPFN when substituting DINOv2 with DINOv3. Results are reported as averaged accuracy over five random seeds.

Encoder	PU20	Mass	Calc	Petfinder
DINOv2	85.22	74.53	75.40	40.74
DINOv3	85.61	75.48	76.75	40.57

Distribution Alignment Across Modalities. We investigate whether applying embedding-space alignment techniques—commonly used in multimodal learning—can further improve the performance of MMPFN. In particular, we incorporate Maximum Mean Discrepancy (MMD) [21], a standard measure of distributional discrepancy [65], into our framework. We apply MMD to the embeddings generated for each feature to reduce the distributional gap between representations from different modalities. For tabular data, where feature distributions can differ substantially across dimensions, we additionally employ Joint MMD (JMMD) [40] to capture discrepancies at the level of the joint feature distribution.

We train the multi-head MLP module that produces unstructured feature embeddings by adding the discrepancy between tabular embeddings and image/text embeddings as an auxiliary loss term. However, as shown in Figure S2, this

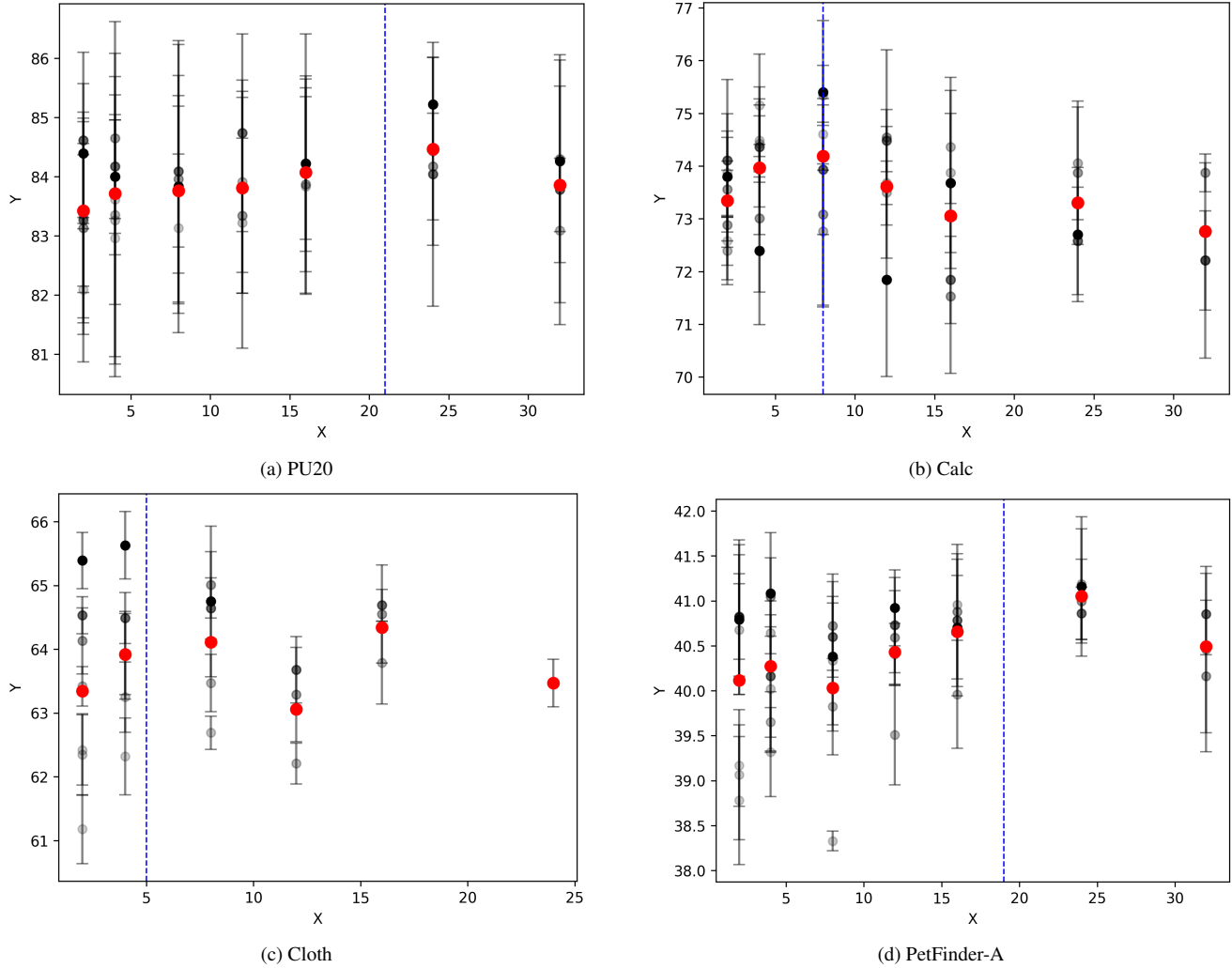


Figure S1. **Effect of the ratio between tabular and non-tabular features.** The black dots and vertical lines show the mean and variance across five random seeds. Darker black dots correspond to a larger number of MGM heads (i.e., more non-tabular features generated by MGM), ranging from 8 to 128. The red dot indicates the average result across all MGM-head settings. The x-axis shows the number of non-tabular features generated by CAP, and the y-axis denotes accuracy. The blue line represents the number of tabular features. Dataset names are shown above each subfigure.

alignment-based regularization consistently underperforms the MGM baseline, and incorporating the same loss directly into MGM also fails to yield improvements. Together with our cosine-similarity analysis, these negative results suggest that embeddings extracted by MGM from image and text modalities are already mapped into a semantically compatible space with tabular embeddings, enabling effective interaction through the attention module. Moreover, while MMD-style losses can reduce distributional gaps, they may also suppress discriminative variations, leading to performance degradation. We therefore infer that once MGM and CAP produce sufficiently aligned embeddings, enforcing additional distributional alignment does not provide further

gains and can even be detrimental.

Comparison with Patch-Token Features In MMPFN, the text encoder [9] and the image encoder [45] produce output embeddings for every token (e.g., text tokens or image patches). In principle, one could replace the $[CLS]$ -based MGM features with ViT patch-token outputs and use all token embeddings directly for feature generation. However, this design has both practical and empirical drawbacks. From a memory perspective, using all patch tokens is substantially more expensive than using the aggregated $[CLS]$ token. For example, when resizing PAD-UFES-20 images to $336 = 14 \times 24$ pixels and encoding them with the

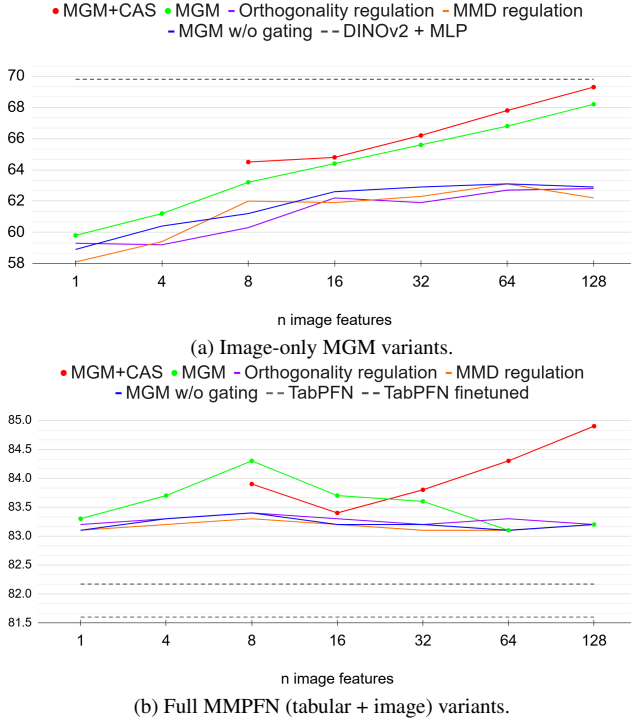


Figure S2. **Effect of distribution-alignment and orthogonality regularization.** Under the same experimental conditions as Fig. 2, we compare the performance of variants that incorporate orthogonality and MMD-based regularization constraints to the MGM baseline, for both image-only and tabular+image settings.

DINOv2 ViT-B/14 backbone, the model produces 576 token embeddings per image—more than four times the number of MGM heads (128) used in our experiments. In terms of storage, the $[CLS]$ embedding requires only 7.1 MB, whereas retaining all patch-token outputs occupies 4.1 GB, leading to a prohibitive increase in memory consumption. A similar issue arises for text: in the Cloth dataset, many text attributes approach the maximum input length of 512 tokens, so storing all token embeddings again results in excessive memory usage.

Empirically, we also observe that models using ViT patch-token outputs underperform those relying on the $[CLS]$ -driven MGM features. On PAD-UFES-20, replacing the $[CLS]$ -based MGM heads with patch-token features decreases accuracy by 0.85 percentage points (from 85.22% to 84.02%). We attribute this degradation to the fact that the $[CLS]$ representation of a well-trained foundation model already encodes task-relevant global information, while raw token-level outputs contain substantial redundancy and noise. Consequently, patch-token features are less suitable than $[CLS]$ -based MGM heads for constructing compact, tabular-like feature representations.

S2. Experiments Setup

Implementation Details. For the training procedure, we adopt the official TabPFN repository² and modify it to support MMPFN by extending the `MMPFNClassifier` and `MMPFNRegressor` classes. Fine-tuning is performed by splitting the available data into training and validation sets and updating model parameters based on the validation loss. We use a small learning rate of 1×10^{-5} , a fixed budget of 100 training steps, and `ScheduleFree` [13] for learning rate scheduling. Fig. S3 shows the learning curve on four different datasets. For contrastive-pretraining baselines [16, 17, 23], we train for 500 epochs using a cosine-annealing scheduler with a 10-epoch warmup.

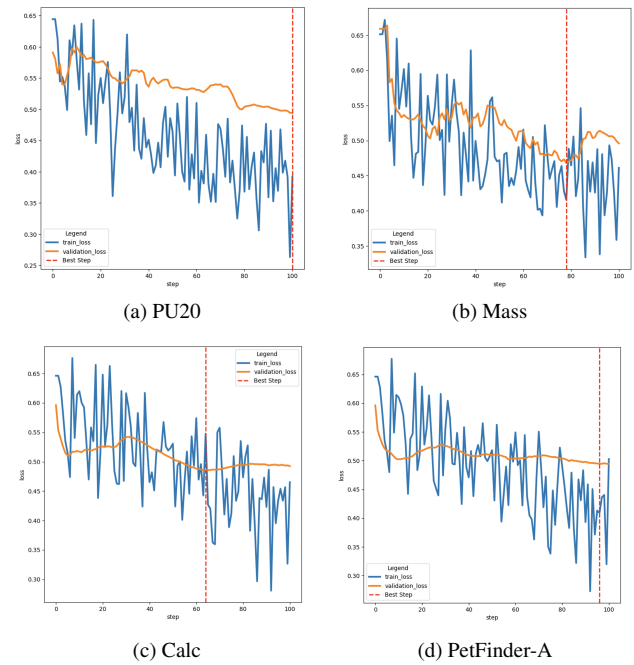


Figure S3. **Fine-tuning loss curves of MMPFN across datasets.** Each subfigure shows the validation loss over training steps for four different datasets, illustrating stable convergence behavior under our fine-tuning setup.

Text Data Pre-Processing. We adopt the text pre-processing pipeline of TTT [5], following the implementations provided in the official codebase. For the Salary dataset, the original source URL referenced in Bonnier [5] is no longer accessible, so we use a Kaggle-hosted copy instead. Applying the official TTT scripts to this version does not reproduce the exact dataset size reported in the paper, suggesting minor discrepancies. We therefore re-evaluate

²https://github.com/LennartPurucker/finetune_tabPFN_v2

the TTT baseline on this revised dataset; the resulting accuracy (46.5) closely matches the originally reported performance, confirming that the new version is suitable for evaluating our model.

Both ELECTRA and DeBERTa text encoders are limited to 512 input tokens, so longer sequences are truncated. For datasets with multiple text attributes, we extract embeddings for each attribute separately and incorporate them as additional text features, whereas TTT concatenates all text columns into a single sequence; this yields small but consistent accuracy gains, although the improvements remain within the error margin and are not reported in the main comparison table. The Airbnb and PetFinder datasets contain Chinese characters in their text fields; because the ELECTRA variant we use is not pretrained on Chinese, these characters are replaced with empty strings before encoding. For CatBoost and AutoGluon, we rely on the libraries' built-in text handling capabilities.

Cosine Similarity Computation. We provide the detailed procedure used for the cosine-similarity-based correlation analysis in Fig. 3 and Sec. 4.3. The TabPFN encoder for tabular data normally groups multiple features into a single embedding to reduce memory usage, but such grouping can introduce noise when comparing cosine similarity between tabular and image (or text) embeddings. To obtain more precise relationships, we set the tabular group size to 1, generate an individual embedding for each feature, and then compare these feature-wise embeddings with image embeddings.

Cosine similarity between input features is computed at the instance level and subsequently averaged across instances. Averaging embeddings over the entire dataset before computing similarity vectors would be cheaper but tends to underrepresent the contribution of individual samples, whereas computing similarity for every token embedding is prohibitively expensive and makes global patterns difficult to visualize. We therefore adopt an intermediate strategy, which balances computational cost and fidelity.